

Low noise laser-based T-ray spectroscopy of liquids using double-modulated differential time-domain spectroscopy

Samuel Peter Mickan^{1,4}, Regina Shvartsman², Jesper Munch³,
Xi-Cheng Zhang² and Derek Abbott¹

¹ Centre for Biomedical Engineering (CBME) and Department of Electrical and Electronic Engineering, The University of Adelaide 5005, Australia

² Center for Terahertz Research and Department of Physics, Applied Physics and Astronomy, Rensselaer Polytechnic Institute, Troy, NY 12180, USA

³ Department of Physics and Mathematical Physics, The University of Adelaide 5005, Australia

E-mail: samuel.mickan@adelaide.edu.au

Received 15 December 2003, accepted for publication 22 March 2004

Published 27 July 2004

Online at stacks.iop.org/JOptB/6/S786

doi:10.1088/1464-4266/6/8/025

Abstract

Liquid transmission studies at terahertz frequencies (0.1–10 THz) are valuable for understanding solvation dynamics of salts, exploring long-range structure in mixtures and probing biomolecules in suspension. T-ray (or THz) time-domain spectroscopy, based on terahertz pulse generation from ultrafast lasers, is a sensitive technique for measuring material parameters in this frequency range. This paper proposes and demonstrates a novel technique for increasing the sensitivity and repeatability of liquid studies with T-ray time-domain spectroscopy (TDS), reducing relative parameter measurement errors below 0.0001. The proposed technique combines dual-thickness liquid measurement with rapid modulation (double-modulated differential TDS) to reduce the effect of both thickness-measurement errors and T-ray noise errors below 0.0001. The possible reduction in error is calculated and a liquid differential TDS (DTDS) prototype is demonstrated, incorporating amplitude and mean detection for near-simultaneous measurement of two T-ray waveforms.

Keywords: Terahertz time-domain spectroscopy (THz-TDS), T-rays, liquid spectroscopy

(Some figures in this article are in colour only in the electronic version)

1. Introduction

The T-ray radiation band lies at the boundary between electronics and photonics, approximately 0.1 to 10 THz. T-rays overlap with high-frequency millimetre waves and the long wavelengths of the far-infrared. T-rays have a diffraction-limited spatial resolution limited by wavelength, λ , to approximately 0.3 mm at 1 THz, which is better than

millimetre (mm) waves, and T-ray Rayleigh scattering is less than for IR light due to its λ^{-4} dependence. The approximate bandwidth of typical pulsed T-ray spectrometers, as used for experiments in this paper, spans from 300 GHz to 3 THz [1–4].

T-rays have a wide range of applications from biosensing [5] through to use in quantum computers [6].

The accuracy of estimating the T-ray frequency parameters of fluids in dual-thickness T-ray spectroscopy is limited by fluctuations in the T-ray pulses, caused by laser fluctuations, and by the accuracy of the thickness measurements [7, 8]. The

⁴ Author to whom any correspondence should be addressed.

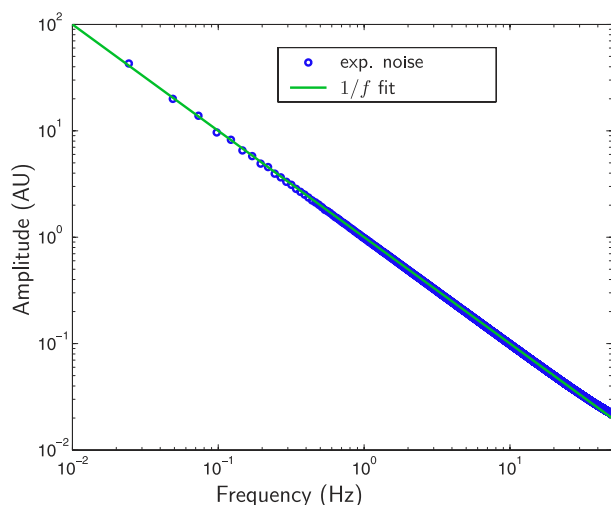


Figure 1. Experimental T-ray noise spectrum. The $1/f$ trend of laser-based T-ray noise is visible in this experimental spectrum. The spectrum is calculated from a set of time-domain measurements of the peak of the T-ray pulse. The 8192 time-domain samples are taken with a time spacing of approximately 5 ms, giving a sample time of 41 s and a measurement frequency range of approximately 0.024–100 Hz. Liquid DTDS would decrease the drift time from approximately 5 min to 0.05 s (0.003–50 Hz), theoretically decreasing the noise caused by laser fluctuations by up to four orders of magnitude.

measurement of thickness change d can be extremely accurate, better than $1:10^4$, using closed-loop feedback control of the mechanism used for changing the material thickness.

Noise in the T-ray beam is caused primarily by laser fluctuations, which are known to have a $1/f$ characteristic, that is, the fluctuation amplitude is greater at lower frequencies. A measured graph of T-ray spectrometer noise is shown in figure 1, where the $1/f$ trend is visible. Normally the two measurements required for material characterization are measured over a period of minutes. The length of time required depends on the signal-to-noise ratio (SNR) of the system. By taking the reference and sample measurements, required in T-ray spectroscopy, at a higher speed, the fluctuation in laser power between measurements is reduced. Rapid thickness modulation, dubbed T-ray differential time-domain spectroscopy (DTDS), has previously been used on thin films [9–11], biosensor slides [5, 12], but not on liquids or gases.

Liquid spectroscopy is best carried out with two thickness measurements, using a thick and a thin portion of liquid. Dual-thickness measurements can be made at higher modulation frequencies by rapidly swapping between the thick and thin portion. This paper describes the theory of the novel technique of liquid DTDS. Experiments with a prototype modulation system based on an audio loud speaker are used to demonstrate the feasibility of liquid DTDS.

1.1. Previous studies

T-ray spectroscopy of fluids has been used to study liquid dynamics, solvation processes and biological systems [13–25]. T-ray fluid parameter studies have been carried out with a variety of spectrometer configurations and parameter

estimation procedures. The experiments in this paper use a dual-thickness geometry, where the sample and reference waveforms are measured through thick and thin versions of the material respectively. Dual-thickness geometry systems have been used by [18] and [8].

In previous work, the typical accuracy of determined parameters is to two decimal places, or worse than 0.1% [14, 21, 25–27]. The work in this paper attempts to improve the accuracy of these measurements by two orders of magnitude.

1.2. Objective

This paper proposes to use double-modulated DTDS to reduce the noise in fluid parameter estimation. In a typical T-ray transmission spectrometer with an SNR of 100:1, each time-domain measurement takes approximately 5 min, and noise is dominated by laser fluctuations ($1/f$). Using a DTDS technique and simultaneous dual waveform acquisition (amplitude and mean detection), the time between measuring the sample and reference waveforms can be reduced to a time determined by the speed of the modulator. Therefore only one delay scan is required to measure both T-ray waveforms, and the time delay between each sample and reference measurement is the inverse of the modulation frequency. For a 10 Hz modulation speed, the increase in effective modulation frequency is 3000 times, and the corresponding decrease in the amplitude of $1/f$ noise is 3000.

2. Theoretical noise reduction

For liquid spectroscopy using a dual-thickness geometry, the accuracy of parameter estimation depends on the fluctuations in the T-ray spectrometer and the accuracy of the thickness change. This section quantifies the benefits of DTDS for characterizing two classes of liquids: those with a low T-ray absorption, for example non-polar solvents, and those with a high T-ray absorption, for example water. The aim is to measure material parameters with an accuracy better than 10^{-4} .

2.1. Dual-thickness theory

The T-ray pulse is modelled as a spectrum of Fourier components, propagating as a plane wave through the material. Figure 2 shows the propagation of radiation through the material, of complex refractive index \tilde{n}_2 , and across two interfaces between the material and the surrounding medium (air), $\tilde{n}_1 \approx 1.0$. The simple equations used for estimating the material parameters are derived from the equations for Fresnel transmission and reflection at interfaces.

A thick piece of material causes sufficient delay so that the transmitted pulse can be measured without any overlap with the first Fabry–Pérot (FP) reflection. The exact requirements for the delay will depend on the desired total scan length. Note that the substrate material both before and after the material under test must also be sufficiently thick to avoid any FP reflections in the measured pulses. Thin substrates are discussed below with thin samples.

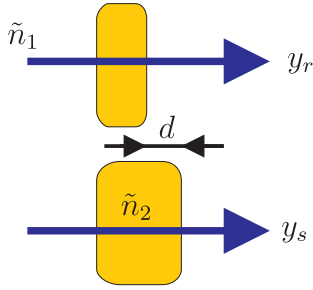


Figure 2. Dual-thickness parameter estimation geometry. The measured T-ray waveforms that pass through the sample (thick) and reference (thin) portions of the material are denoted y_s and y_r , respectively. The spectral components S of the waveforms are determined by a FFT (fast Fourier transform) of the waveforms y : $\tilde{S}_s = \mathcal{FT}(y_s)$ and $\tilde{S}_r = \mathcal{FT}(y_r)$. The difference in thickness between the two measurements is denoted d .

For a thick material, the experimentally measured spectral components of the reference and sample pulses can be modelled by [4, 28, 29]

$$\tilde{S}_r(\omega) = A(\omega)t_{12}p_{d_{\text{thin}}}t_{21}, \quad \tilde{S}_s(\omega) = A(\omega)t_{12}p_{d_{\text{thick}}}t_{21}, \quad (1)$$

where \tilde{S}_r and \tilde{S}_s are spectral components of the reference (subscript r) and sample pulses (subscript s) shown in figure 2, t_{ab} and p_{d_*} are the transmission and propagation coefficients of a plane THz wave (defined below—the subscripts refer to transmission from material \tilde{n}_a to material \tilde{n}_b , and propagation through material of thickness d_* , where ‘*’ stands for either *thick* or *thin*), and $A(\omega)$ is the product of all other system responses that remain constant between the sample and reference measurements. For an interface between two media of refractive indices \tilde{n}_a and \tilde{n}_b , oriented normal to the radiation path, the plane wave transmission (t) and reflection (r) coefficients simplify to [28, 30]:

$$t_{ab}(\omega) = \frac{2\tilde{n}_a}{(\tilde{n}_a + \tilde{n}_b)}, \quad \text{and} \quad r_{ab}(\omega) = \frac{\tilde{n}_a - \tilde{n}_b}{\tilde{n}_a + \tilde{n}_b}. \quad (2)$$

Radiation propagating a distance d_a through a linear medium, \tilde{n}_a , is delayed and attenuated according to the factor

$$p(\omega) = e^{-j\tilde{n}_a\omega d/c_0}, \quad (3)$$

where c_0 is the speed of light in a vacuum.

The ratio of the transmission spectra can thus be entirely determined in terms of refractive indices and the material thickness [8, 28, 30],

$$\tilde{T} = \tilde{S}_s/\tilde{S}_r = \frac{e^{-j\tilde{n}_2\omega d_{\text{thick}}/c_0}}{e^{-j\tilde{n}_2\omega d_{\text{thin}}/c_0}e^{-j\tilde{n}_1\omega(d_{\text{thick}}-d_{\text{thin}})/c_0}}, \quad (4)$$

where \tilde{n}_1 is the material that replaces the space taken up by the extra thickness of the thick piece of material, typically air.

Equation (4) simplifies to

$$\tilde{T} = \exp(-j\omega d(\tilde{n}_2 - 1)/c_0), \quad (5)$$

where $d = d_{\text{thick}} - d_{\text{thin}}$ and $\tilde{n}_1 = 1$. Since \tilde{T} is complex, $\tilde{T} = \rho e^{j\phi}$, and $\tilde{n} = n - j\kappa$,

$$\rho = \exp(-\omega d\kappa/c_0), \quad \phi = -\omega d(n_2 - 1)/c_0. \quad (6)$$

The material parameters can then be extracted by rearranging the above equations [31],

$$n = \frac{-\phi c_0}{\omega d} + 1, \quad \kappa = -\ln(\rho) \frac{c_0}{\omega d}. \quad (7)$$

These calculations provide a value for the T-ray refractive index n and extinction coefficient κ of the mixture. The values of \tilde{S}_s and \tilde{S}_r are measured by taking the Fourier transform of the transmitted time-domain T-ray pulses, y_s and y_r , respectively. The accuracy of equation (7) depends only on the accuracy of d and on the noise of the T-ray spectrometer signal, $\delta\rho$ and $\delta\phi$.

2.2. Uncertainty

The accuracy of equation (7) depends only on the noise of the T-ray spectrometer, $\delta\phi$ and $\delta\rho$, and on errors in the translation stage measurement δd . The influence of errors on the parameter of interest (\tilde{n}) can be estimated using the partial derivatives:

$$\delta n = \delta n_d + \delta n_\phi, \quad \delta \kappa = \delta \kappa_d + \delta \kappa_\rho, \quad (8)$$

where

$$\begin{aligned} \delta n_d &= \frac{\partial n}{\partial d} \delta d = \frac{\phi c_0}{\omega} \frac{1}{d^2} \delta d, \\ \delta \kappa_d &= \frac{\partial \kappa}{\partial d} \delta d = \frac{\ln(\rho) c_0}{\omega} \frac{1}{d^2} \delta d, \\ \delta n_\phi &= \frac{\partial n}{\partial \phi} \delta \phi = -\frac{c_0}{\omega d} \delta \phi, \\ \delta \kappa_\rho &= \frac{\partial \kappa}{\partial \rho} \delta \rho = -\frac{c_0}{\omega d} \frac{\delta \rho}{\rho}. \end{aligned} \quad (9)$$

The T-ray noise comes from three main sources: (i) the T-ray emitter, (ii) the T-ray detector and (iii) the probe beam. The noise in the emitter dominates and is multiplicative, that is, proportional to the signal strength. The noise in the probe beam is additive, that is, independent of signal strength, and only dominates when the signal strength is low. For experiments dominated by multiplicative noise, that is, noise due to fluctuations in the T-ray signal (pump beam) rather than noise in the detection system (probe beam) [32], the phase error is approximately equal in both the sample and reference spectra,

$$\delta \phi_s \approx \delta \phi_r. \quad (10)$$

From $\phi = \phi_s - \phi_r$ and equation (10), $\delta \phi \approx 2\delta \phi_r$.

For uncorrelated additive noise in both the sample and reference, the combined effect of noise in both sample and reference can be estimated from

$$\frac{\langle \delta \rho^2 \rangle}{\rho^2} = \frac{\langle \delta \rho_r^2 \rangle}{\rho_r^2} + \frac{\langle \delta \rho_s^2 \rangle}{\rho_s^2}. \quad (11)$$

For multiplicative noise, the relative amplitude error is similarly approximately equal in both the sample and reference spectra, giving

$$\frac{\delta \rho}{\rho} \approx \sqrt{2} \frac{\delta \rho_r}{\rho_r}, \quad (12)$$

$$\delta \rho = \frac{\sqrt{2} \exp(-\frac{\omega d \kappa}{c_0})}{\rho_r} \delta \rho_r. \quad (13)$$

Using equation (6), and the relations for uncorrelated noise sources,

$$\langle \delta n^2 \rangle = \langle \delta n_d^2 \rangle + \langle \delta n_\phi^2 \rangle, \quad \langle \delta \kappa^2 \rangle = \langle \delta \kappa_d^2 \rangle + \langle \delta \kappa_\rho^2 \rangle, \quad (14)$$

expressions for the uncertainty in measurements due to phase, amplitude and thickness uncertainties are obtained:

$$\delta n = \frac{n-1}{d} \sqrt{\left(\frac{2c_0 \delta \phi_r}{\omega(n-1)} \right)^2 + (\delta d)^2}, \quad (15)$$

$$\delta \kappa = \frac{\kappa}{d} \sqrt{\left(\frac{\sqrt{2}c_0 \delta \rho_r}{\omega \kappa \rho_r} \right)^2 + (\delta d)^2}. \quad (16)$$

The uncertainty in the estimation of refractive index and extinction coefficient can be predicted from the inherent noise in the T-ray spectrometer, T_r , and the accuracy of the thickness modulator.

To study the influence of these uncertainties, we look at four cases: (i) δd dominant in a low- κ material (for example, a non-polar solvent); (ii) $\delta \rho$ and $\delta \phi$ dominant in a very thick low- κ material; (iii) δd dominant in a high- κ material (for example, water); (iv) $\delta \rho$ and $\delta \phi$ dominant in a high- κ material.

2.2.1. δd dominant in low- κ . For noise dominated by errors in d , equations (15) and (16) can be simplified by ignoring the first term in the square root, giving

$$\delta n = (n-1) \frac{\delta d}{d}, \quad \delta \kappa = \kappa \frac{\delta d}{d}. \quad (17)$$

Equation (17) indicates that noise can be reduced by using a large thickness change d compared to the thickness measurement error δd . Notice that δd is limited by the actuator resolution. A ratio of $\frac{\delta d}{d} < 10^{-4}$ can be achieved by using, for example, a 5 mm distance change between thicknesses and 0.4 μm stage resolution, or a 30 μm piezoelectric stage with 1 nm resolution. An accuracy of 10^{-4} would constitute an improvement of 100 times over most previous T-ray liquid characterization results. Such high-accuracy mechanical modulators are commercially available.

Since it is easy to use a modulator that will contribute a relative noise of only 1 part in 10 000, the dominant source of noise is typically spectrometer noise, $\delta \rho$ and $\delta \phi$. Systems dominated by spectrometer noise are discussed in sections 2.2.2 and 2.2.4.

2.2.2. $\delta \rho$ and $\delta \phi$ dominant in low- κ . For errors dominated by noise in the T-ray beam, equations (15) and (16) can be simplified by ignoring the second term in the square root, giving

$$\delta n = \frac{2c_0 \delta \phi_r}{\omega d}, \quad \delta \kappa = \frac{\sqrt{2}c_0 \delta \rho_r}{\omega d \rho_r}. \quad (18)$$

These equations can be understood by substituting approximate values from a typical T-ray spectrometer measurement. For example, $\omega = 6.3 \times 10^{12}$ at a frequency of 1 THz, and $\rho_r = 0.655$, $\delta \rho_r = 0.015$ and $\delta \phi_r = 0.025$ rad for a scan of the organic solvent 1,4-dioxane, using the liquid T-ray spectrometer from section 3. In this measurement, the

LIA (lock-in amplifier) time constant is 100 ms, giving a scan duration of approximately 5 min. Using these numbers,

$$\delta n \approx \frac{5 \times 10^{-6}}{d}, \quad \delta \kappa \approx \frac{3 \times 10^{-6}}{d}. \quad (19)$$

From equation (19) it can be seen that an accuracy of 10^{-4} is achievable at this noise level (100 ms LIA time constant and 5 min scan) by using an approximate thickness change of $d > 10$ mm. This large thickness change is possible with large volumes of liquid with a low T-ray absorption. If, however, the T-ray absorption of the liquid is not very low, a 50 mm-thick piece of material will attenuate the T-rays too greatly to be detected. For high- κ materials, the initial noise in the T-ray signal must be reduced to compensate for the necessity of a small thickness change.

2.2.3. δd dominant in high- κ . For high- κ materials, the uncertainty caused by δd is governed by the same equations as for low- κ materials, equation (18). For a highly absorbing liquid, however, it is not possible to use a 5 mm distance change. The thickness modulation must be less than 100 μm and be measured with a very high accuracy, using for example a piezoelectric translator.

2.2.4. $\delta \rho$ and $\delta \phi$ dominant in high- κ . For high- κ materials, δn is greatly attenuated, and $\delta \rho$ is dominated by additive noise. Thus

$$\delta \kappa = \frac{\sqrt{2}c_0}{\omega d} \frac{\delta \rho_s}{\exp\left(\frac{-\omega d \kappa}{c_0}\right)} \approx \frac{1.3 \times 10^{-4}}{d} \delta \rho_s \frac{1}{\rho}. \quad (20)$$

The error is proportional to $1/\rho$. We can compare the influence that increasing the modulation thickness, d , has on the accuracy of our estimations when using two different liquids, dioxane ($\kappa_{\text{dioxane}} = 0.013$) and water ($\kappa_{\text{water}} = 0.478$). The graph in figure 3 shows that the error in κ measurements of a high- κ liquid, water, increases with the material's thickness. For a low- κ liquid, dioxane, the error decreases with increasing thickness.

Figure 3 shows that a thickness change of even 1 mm generates a very high error in a high- κ liquid, thus limiting experiments to sub-millimetre modulation.

2.2.5. Summary. From the foregoing analysis of uncertainty, we see the best modulation system for liquid spectroscopy depends on the properties of the liquid. For a low- κ liquid, a high accuracy can be achieved by using a very large thickness change up to $d = 10$ mm. For a high- κ liquid, only a small thickness change is possible, and the errors must be reduced in two ways: (i) the thickness change must be accurate, for example, by using a piezoelectric translator, and (ii) the inherent noise in the T-ray signal must be reduced, by using for example high-frequency thickness modulation in double-modulated DTDS.

For dioxane measurements, an accuracy of $\sim 10^{-4}$ is desirable. From equation (19), a thickness change of ~ 10 mm is required, with a resolution of 1 μm . Since dioxane has low absorption, this is possible.

For water measurements, a thickness of 1 cm is unusable since the T-ray absorption is too high. A thickness change of around 100 μm and a resolution of 10 nm is required, using for example a piezoelectric actuator.

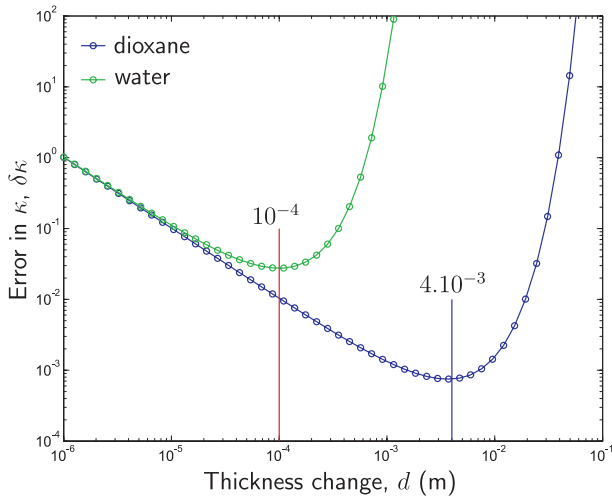


Figure 3. Plot of $\delta\kappa$ versus d . The two liquids in the graph are dioxane, $\kappa = 0.013$, and water, $\kappa = 0.478$. For the typical error in a T-ray spectrometer, for example $\delta\rho_s = 0.015$, the error in the estimation of the κ parameter depends on the thickness change d of the material. The error decreases for larger thickness change, from equation (20), but for highly-absorbing liquids, such as water, the absorption of the thicker extreme masks the T-ray signal. These plots show the approximate thickness change desirable for minimum error. For dioxane, a greater change is desirable, approximately 4 mm. For water, the optimal thickness change is much less, approximately 100 μm .

3. Experiment

This section describes an initial experimental verification of the accuracy of liquid DTDS and discusses its limitations.

The experimental implementation of liquid DTDS involves three main elements:

- (i) a standard T-ray transmission spectrometer,
- (ii) a holder for modulating the liquid material at a modulation frequency f_2 , and
- (iii) electronic signal processing to extract the sample and reference waveforms, y_s and y_r .

The spectrometer used in these experiments is the same system used in standard liquid transmission spectroscopy [7, 8], and is shown schematically in figure 4.

The liquid holder needs to provide a rapid transition between a thick and thin material, corresponding to y_s and y_r in dual-thickness spectroscopy. In the prototype system this is implemented using one large fixed Teflon window and one moving window mounted on an audio speaker, as shown in figure 5. The speaker is driven by a square wave to switch between the thick and thin positions. The signal processing consists of two parts: the standard DTDS double de-modulation [10, 33] to extract the difference waveform $y_d = y_s - y_r$, and a second part to measure the mean waveform $y_m = y_s + y_r$. *Amplitude and mean detection* is described in section 3.1.

The two Teflon windows, held perpendicularly to the T-ray beam axis, are thicker than 10 mm to avoid Fabry–Pérot reflections in the recorded waveform. Teflon is a good material for T-ray windows because of its low refractive index and low absorption. The actual liquids are held in a high-density polyethylene bag (HDPE), a material that does not dissolve in the solvent. HDPE has a low T-ray refractive index and low T-ray absorption. With an average wall thickness less than

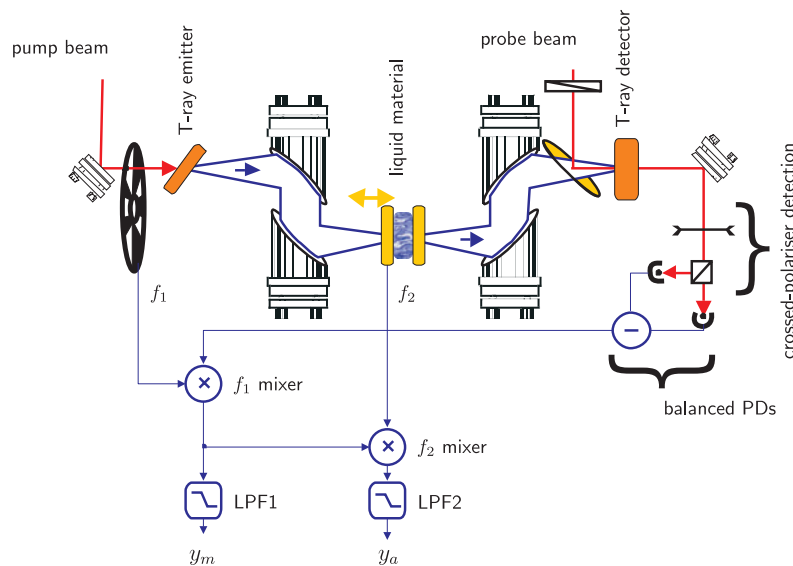


Figure 4. Liquid DTDS spectrometer schematic. This schematic depicts a standard T-ray spectrometer configured for characterizing a liquid. In liquid DTDS the thickness of the material is modulated dynamically at a frequency f_2 , and the electronic demodulation is similar to thin film double-modulation DTDS [10, 33]. The Ti:sapphire mode-locked (ML) laser generates a train of 100 fs pulses at 82 MHz. Each pulse is split into a pump beam and a probe beam. The pump beam generates T-ray pulses when incident at Brewster’s angle on the GaAs wafer, positioned at the focal point of a gold-coated parabolic reflector. Parabolic reflectors collimate the T-rays, focus it into the liquid holder, then collect the transmitted radiation and direct it into a $\langle 110 \rangle$ ZnTe T-ray detector. The probe beam detects the T-ray electric field in the ZnTe, and is in turn recorded with crossed polarizers and balanced photodetectors. The thickness of the material is modulated with two Teflon windows, one of which is mounted on a manual translation stage. The mixture is held in a sealed, thin-walled, high-density polyethylene (HDPE) bag, which does not react with or dissolve in dioxane. The measured mean and amplitude waveforms (defined in section 3 and shown in figure 7) are denoted y_m and y_d , respectively.

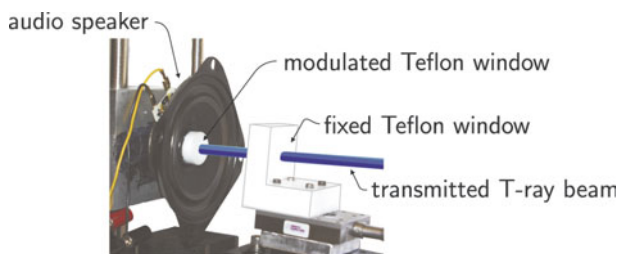


Figure 5. Photograph of the prototype liquid DTDS holder. This photograph shows the two windows used to control the thickness of a liquid in liquid DTDS, that is the fixed window and the modulated window attached to a speaker. The speaker is a 4 inch-diameter mid-range speaker, with 8Ω DC coil resistance. There is a hole drilled in the back end of the speaker to allow transmission of the T-rays. The speaker is driven by a square wave of frequency f_2 from an SRS signal generator (DS340), and travels axially along the T-ray beam propagation direction. The T-ray beam is drawn in this figure for clarity although it is not visible to the human eye.

0.1 mm thick, less than the majority of T-ray wavelengths, and a very low refractive index mismatch between Teflon and HDPE, etalon effects from the plastic bag walls are negligible. Experimentally, no multi-reflections are observed in the measured pulses. For a low mismatch between \tilde{n}_1 , \tilde{n}_2 and \tilde{n}_3 , and a thin bag wall, the influence of etalon effects is slight.

3.1. Amplitude and mean detection

Amplitude and mean detection is an electronic technique that enables the simultaneous measurement of both the sample and reference waveforms when a material is modulated in the T-ray beam. Amplitude and mean detection can be used in any DTDS experiment and is implemented as part of the signal detection electronics. In amplitude and mean detection, instead of discarding 50% of the y_d waveform as in double-modulated DTDS [10, 11, 33], half the signal is used to simultaneously measure y_r . The advantage of this is that the hardware requires no modification from double-modulated DTDS and that the time between measuring y_d and y_r is reduced from the order of minutes to the order of milliseconds. For measurements dominated by $1/f$ noise, a reduction in the scan-to-scan delay time increases the SNR, potentially by several orders of magnitude.

A mean and amplitude detection system can be implemented in stand-alone electronics, using a fast analogue-to-digital converter ($\gg f_1$) and two stages of digital demodulation, synchronized with the movement of the delay stage. The diagram in figure 6 shows schematically how the double-modulated signal from the photodiodes is demodulated in two stages. The double demodulation process can be understood in the time domain by looking at the square waveform detected by the photodiodes as the material is modulated differentially. An example detected waveform is shown in figure 7, showing how y_m and y_a relate to y_s and y_r at the output of the first mixer.

It is possible to simultaneously record the sample and reference waveforms in one scan when the material is being dithered in and out of the T-ray beam, as in DTDS. In order to measure both y_s and y_r at a modulation frequency of f_2 , two values are found for each delay point, and as the delay

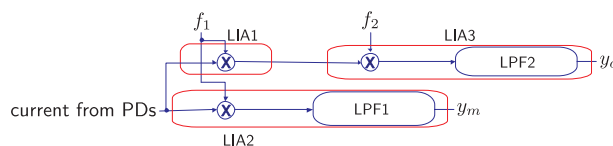


Figure 6. Schematic of mean and amplitude detection. The double-modulated signal from the balanced photodiodes (PDs) is demodulated in two stages. The first demodulation by the higher frequency f_1 is followed by a narrow band low-pass filter LPF1. The second demodulation by the low frequency f_2 is again followed by the narrow band LPF2. $y_r = y_m - y_a$ and $y_s = y_m + y_a$. Experimentally, each of the blocks shown can be implemented with a LIA (lock-in amplifier) and the bandwidth of the LPFs are determined by the time constants of the LIAs. LIA1 acts as the f_1 demodulator and LIA2 acts as the amplitude detector with a long time constant (approximately 100 ms), demodulating at f_2 . A third LIA, LIA3, also with a longer time constant (100 ms) acts as a f_1 demodulator and detects the mean waveform. No low-pass filtering is required in LIA1, so its bandwidth is set very broad (30 μ s time constant).

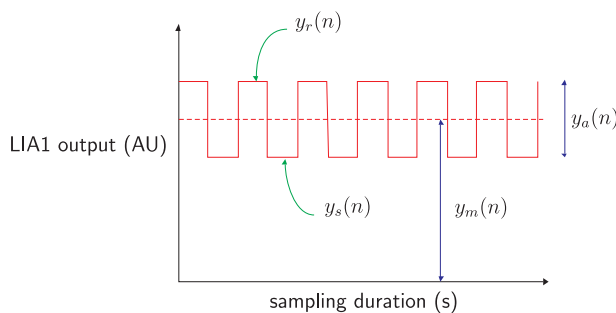


Figure 7. Amplitude and mean detection at one delay point. This figure shows the output of the first demodulator (for example, a lock-in amplifier, LIA1) being modulated by the sample modulation (for example, changing the liquid thickness). This is the time-domain waveform seen for the n th step of the delay stage. The relationship between y_m , y_a , y_s and y_r can be seen in the diagram. The errors arising from amplitude and mean detection are caused by deviations of the observed signal from an ideal square wave, and this depends on the physical constraints of the system, as discussed in section 2.2.

stage moves (figure 4), two waveforms are plotted, y_m and y_a . At each point of the scanning delay line, first the reference signal is measured, then the sample signal. This can be done by having the material on a dithering mechanism, as in DTDS. The T-ray beam is modulated at an audio frequency f_1 and the material is dithered at some low frequency, f_2 . For example, $f_1 = 2$ kHz and $f_2 = 10$ Hz. In double-modulated DTDS, the f_1 carrier frequency is demodulated and the amplitude of f_2 waveform is monitored. As mentioned above, this is in fact the difference between the two waveforms. By using an integrator (low-pass filter), we can simultaneously monitor the mean value of the 10 Hz square wave, which gives (half) the sum of the two waveforms. The mean is the standard output of the first LIA (lock-in amplifier) in figure 6. The amplitude is the output of the second LIA used in double-modulated DTDS. Thus y_r and y_s can be calculated at each point in the same time that it takes to do a normal DTDS scan.

The experiment can be realized with an anti-aliasing filter, a local oscillator referenced to f_1 , a local oscillator referenced to f_2 and an integrator, as shown in figure 6. In the experimental work described in this paper, the system

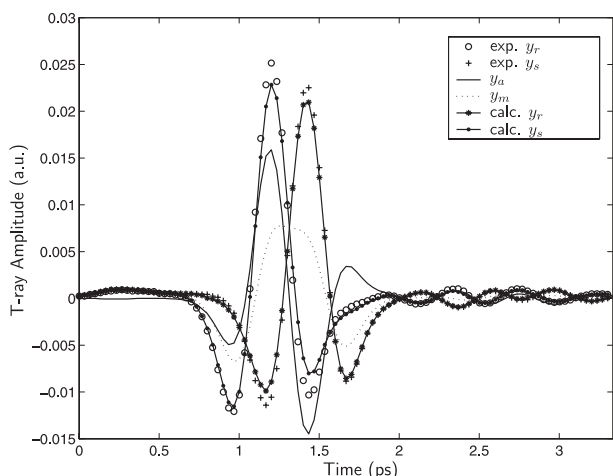


Figure 8. Amplitude and mean detection. Example of single-scan DTDS. The waveforms y_m and y_a are measured with double-modulated DTDS, using the system shown in figure 6. The ‘calc. y ’ waveforms are calculated from $y_r = y_m - y_a$ and $y_s = y_m + y_a$. The two waveforms ‘exp. y_r ’ and ‘exp. y_s ’ are measured using the same T-ray spectrometer configuration and material to be tested, but without modulating the material and taking two separate sample and reference scans (normal T-ray TDS). The match between ‘calc. y ’ and ‘exp. y ’ is an experimental confirmation that amplitude and mean detection provide exactly the same information about a piece of material as normal T-ray TDS, but with a potentially far lower noise level.

is implemented with three LIAs. The same effect could be achieved digitally with a low-noise preamplifier, a fast analogue-to-digital converter and a dedicated processor. The factors of two are missing in figure 6 because y_r and y_s are effectively halved by dithering the material. The trade-off is that although the signal level is halved, the two waveforms are measured in the same period of time.

Figure 8 experimentally demonstrates the technique of mean and amplitude detection in the T-ray spectrometer. The mean and amplitude waveforms are taken as shown in figure 6, which effectively means the outputs of the second and third LIAs, respectively. The accuracy of the technique is confirmed by comparing the calculated waveforms, from $y_r = y_m - y_a$ and $y_s = y_m + y_a$ using amplitude and mean data, to two waveforms measured using normal T-ray TDS, ‘exp. y_r ’ and ‘exp. y_s ’. The slight difference between ‘calc. y_r ’ and ‘exp. y_r ’ in figure 8 is due to the holder being modulated by an imperfect square wave. This is a mechanical error introduced by the prototype mechanical modulation arm [10].

4. Results

The results for a preliminary demonstration of liquid DTDS show that liquid spectroscopy is functional, and show the technique’s limitations. The difference waveform y_d is shown experimentally to be equal to $y_r - y_s$, as required for the DTDS analysis. The accuracy of the measurements, which is critical to accurate material characterization, is shown to depend on the static linearity of the actuator (audio speaker), the dynamic non-linearities introduced at higher modulation frequencies and larger modulation amplitudes. The goal in a liquid DTDS system is to have as large a movement as possible at as

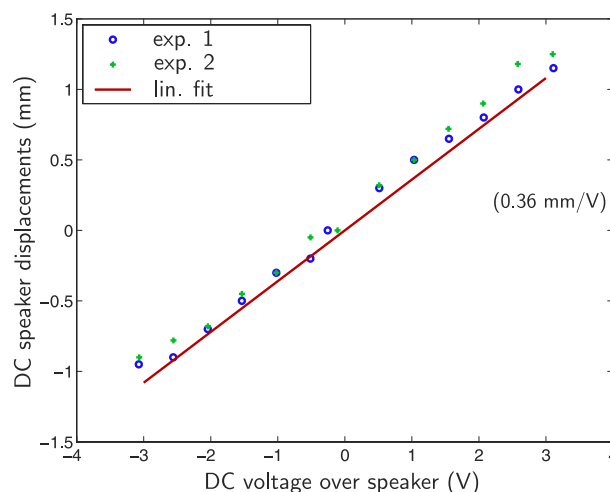


Figure 9. DC linearity of speaker displacement. DC linearity of the 4 inch RCA mid-range speaker. This data is determined manually using a micron-resolution manual stage to measure the displacement at each different DC bias voltage. The two measured plots give an indication of the repeatability of the speaker’s motion. The linear plot gives an indication of the linearity of the speaker.

high a frequency as possible. A large movement (thickness change d) increases the accuracy of the parameter estimation (section 2). A higher modulation frequency allows for less $1/f$ fluctuation. The best possible modulation amplitude and frequency depends on mechanical limitations of the holder, as seen in the following results.

4.1. Displacement calibration

For DC driving voltages, the speaker is found to have a displacement versus voltage characteristic shown in figure 9. The displacement is essentially linear for nominal driving voltage = -3.0 to $+3.0$ V, with a slope of approximately 0.36 mm V^{-1} . The error in displacement measurements, $\delta d \approx 0.05 \text{ mm}$. The displacement to displacement error ratio, $\delta d/d$ can dominate uncertainty in parameter estimation, and therefore must be minimized (section 2). For accurate material characterization, linearity is required to create a mechanical square wave (figure 7), and repeatability is required for high accuracy.

The DC characteristics of the speaker are less important than its AC, or dynamic, characteristics. The most important feature of the system’s dynamic characteristics is that it accurately provides a square-wave motion, and therefore a y_d (and y_m) is accurately detected. This accuracy can be estimated by comparing a normal TDS difference measurement, $(y_r - y_s)/2$, to a DTDS measurement y_d . The accuracy is quantified by the spectral ratio of the two measurements over a certain frequency range where the T-ray signal is strong, for example 0.3 to 1.1 THz .

To experimentally determine the best modulation amplitude and frequency, measurements of y_s , y_r and y_d are taken with the T-ray spectrometer and a mixture of anhydrous hexanes (approximately 10 mL in the HDPE bag).

Figure 10(a) shows the experimentally measured accuracy of the DTDS measurements for increasing modulation frequency. The modulation frequency is limited to a range

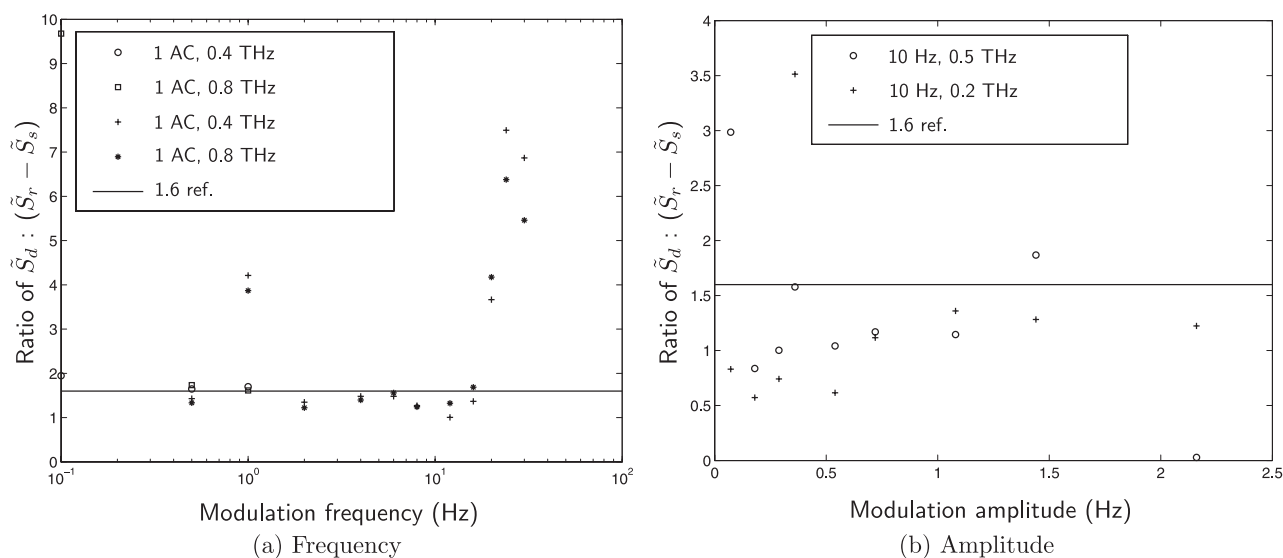


Figure 10. Optimal modulation frequency and amplitude. These graphs show how the accuracy of liquid DTDS is optimal for a limited range of modulation frequency and amplitude. The *ref* line indicates a ratio 1.6, which means the DTDS measurement is 100% accurate. All measurements are made with a displacement amplitude of 1 V AC. This data is measured with a mixture of anhydrous hexanes, chosen for its low T-ray absorption. In (a), the plots for 0.4 and 0.8 THz are spectral components extracted from the pulsed waveforms; the plots for different T-ray frequencies have similar responses to the modulation frequency.

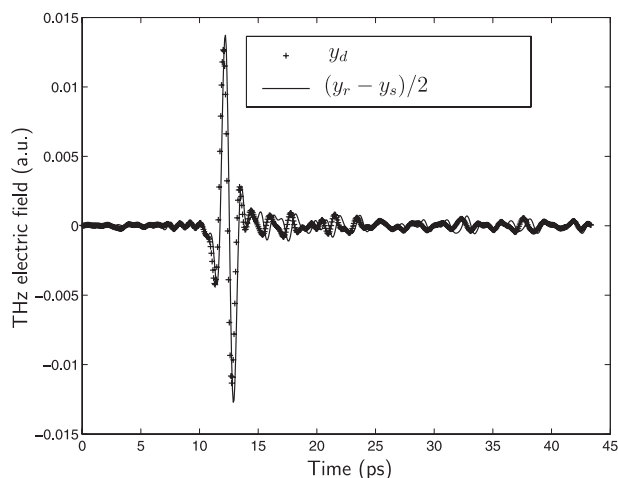


Figure 11. DTDS y_d and $(y_r - y_s)/2$. Comparison of y_d and $(y_r - y_s)/2$. The waveforms have been smoothed with a bandpass filter set at T-ray frequencies with highest SNR.

of approximately $2 < f_3 < 10$. These measurements are all made at a modulation amplitude of 1 V AC. The *ref* line indicates a ratio of 1.6, which is expected between $(y_r - y_s)/2$ and y_d . Using double modulation, we expect the amplitude of

$$y_d = A(y_r - y_s) \quad (21)$$

where $A = 0.5 \times 0.6$. The factor of 0.5 arises from double modulation, and the factor of 0.6 accounts for the LIA measuring only the fundamental sine component of the actual square wave. These results indicate a maximum modulation frequency of about 10 Hz for this hardware.

The accuracy of DTDS measurements at different amplitudes is measured using the same organic solvent (an anhydrous mix of hexanes) and a 10 Hz modulation frequency.

Table 1. Error sources in liquid DTDS. Typically in a spectroscopy experiment, the following values are found for 0.5 THz. For repeatability of the T-ray spectrum, $\phi = 22.30$, $\delta\phi = 0.037$, $\rho = 0.67$ and $\delta\rho = 0.020$. For the thickness accuracy with $d = 1.6$ mm, a manual estimate has $\delta d = 5 \mu\text{m}$ and a DTDS estimate has $\delta d = 0.1$ mm, limited by the audio speaker. These results come from actual measurements of anhydrous dioxane. The error estimates are calculated using the equations in section 2.2.

Noise source	Parameter	Final error	Translation method
Due to δT	δn	0.0044	TDS
	$\delta\kappa$	0.0025	TDS
Due to δd	δn	0.0042	TDS
		0.083	DTDS
	$\delta\kappa$	0.000075	TDS
		0.0015	DTDS

The displacement amplitude d is limited to about 2.2 mm. Figure 10(b) shows the highest accuracy of the DTDS measurements occurs at a displacement of 1.6 mm.

The most accurate measurements are taken at 10 Hz with a displacement of 1.6 mm. Figure 11 shows a direct comparison of the waveforms from DTDS (y_d) and normal TDS. The large overlap of the waveforms experimentally verifies equation (21).

The biggest problem with this system is the inaccuracy in the displacement measurements. The error due to δd is far greater than the error due to δT . For example, table 1 shows approximate error levels for typical spectroscopy measurements. The greatest source of error comes from inaccuracies in the measurement of d . The mechanical displacement accuracy can be greatly increased using a number of methods, including real-time external displacement measurement and closed-loop control. One method of achieving a very low δd is to use a piezo translation system, as discussed in section 5.

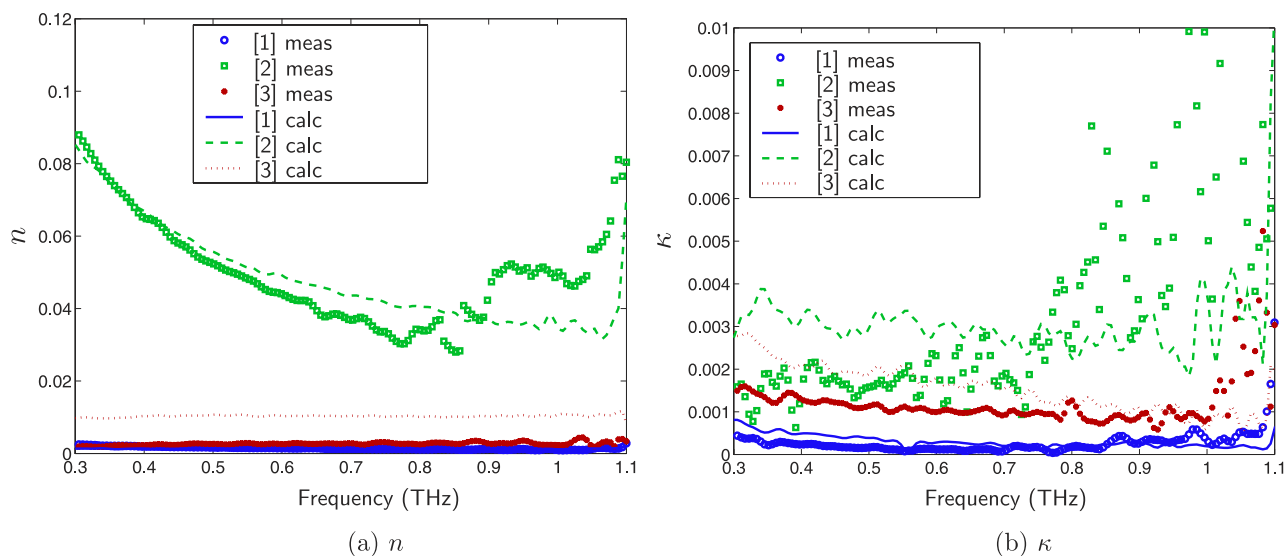


Figure 12. Experimental uncertainties. The uncertainties are estimated with MATLAB's standard deviation function from six repeated experimental measurements. The points represent the standard deviation of the estimated values. The lines represent equation (19). The three liquids are: (i) anhydrous dioxane, (ii) dioxane and water, and (iii) dioxane and a protein suspension (SC).

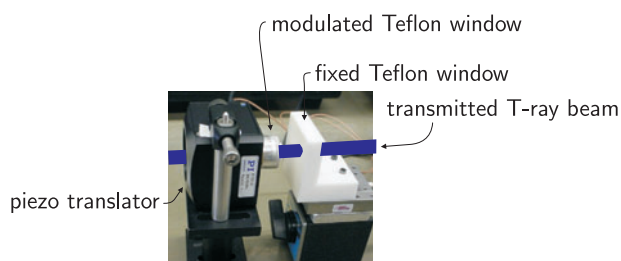


Figure 13. Piezoelectric liquid modulator. The modulated Teflon window is driven by a piezoelectric microscope objective positioner. The positioner has a travel of 350 μm , closed-loop resolution of 10 nm and a loaded resonant frequency of 100 Hz. It will be used to characterize highly-absorbing liquids. The mechanical noise will be far less than that of the audio speaker modulator. The T-ray beam is drawn in this figure for clarity although it is not visible to the human eye.

4.2. Experimental examples of uncertainty

To confirm the equations of section 2.2, this section describes the experimental repeatability and estimated uncertainty in actual dual-thickness experiments. Six T-ray TDS measurements of anhydrous dioxane are taken and the standard deviation is estimated using MATLAB. Then equation (19) is used to calculate the predicted uncertainty. The calculated uncertainty spectrum is shown in figures 12(a) and (b). The actual uncertainty in a series of measurements can be estimated from the standard deviation of a series of estimated values of n and κ . As shown in figures 12(b) and (a), the equations provide an accurate estimate or an over-estimation of the error. These results confirm the accuracy of the equations used above to quantify the sources of uncertainty.

5. Conclusion

The results demonstrated a novel implementation of double-modulated DTDS for liquid spectroscopy. The prototype

system confirmed a reduction in noise at an increased modulation frequency, and confirmed the accuracy of equation (19). The main limitation of the prototype is the dominant mechanical noise at higher modulation frequencies and amplitudes.

In future work the liquid holder system will be implemented using a piezo-electric driven Teflon window. The advantage of a piezoelectric modulator is the extreme accuracy of movement, with $\delta d/d$ better than 10^{-4} . A photograph of the proposed piezoelectric modulator is shown in figure 13.

Acknowledgments

We would like to acknowledge support from the US National Science Foundation, the US Army Research Office, the Australian Fulbright Commission, Clough Engineering (Perth, Australia) and the Australian Research Council.

References

- [1] Mickan S P, Abbott D, Munch J, Zhang X-C and van Doorn T 1999 Analysis of system trade-offs for terahertz imaging *Electronics and Structures for MEMS (Gold Coast, QLD, Australia, 1999)*; *Proc. SPIE* **3891** 226–37
- [2] Mickan S P, Abbott D, Munch J, Zhang X-C and van Doorn T 2000 Analysis of system trade-offs for terahertz imaging *Microelectron. J.* **31** 503–14
- [3] Siegel P H 2002 Terahertz technology *IEEE Trans. Microw. Theory Tech.* **50** 910–28
- [4] Mickan S P and Zhang X-C 2003 T-ray sensing and imaging *Terahertz Sensing Technology: Electronic Devices & Advanced Technology (Selected Topics in Electronics and Systems)* ed D Woolard, M S Shur and W Leorop (Singapore: World Scientific) pp 251–326
- [5] Mickan S P, Menikh A, Liu H, Mannella C A, MacColl R, Abbott D, Munch J and Zhang X-C 2002 Label-free bioaffinity detection using terahertz technology *Phys. Med. Biol.* **47** 3789–96
- [6] Cole B E, Williams J B, King B T, Sherwin M S and Stanley C R 2001 Coherent manipulation of semiconductor quantum bits with terahertz radiation *Nature* **410** 60–3

- [7] Mickan S P, Dordick J S, Munch J, Abbott D and Zhang X-C 2002 Pulsed THz protein spectroscopy in organic solvents *Conf. on Lasers and Electro-Optics '02 (Long Beach, CA, USA)* (Bellingham, WA: SPIE Optical Engineering Press) p 640
- [8] Mickan S P, Dordick J S, Munch J, Abbott D and Zhang X-C 2002 Terahertz spectroscopy of bound water in nano suspensions *Biomedical Applications of Micro- and Nanoengineering (Melbourne, Australia, 2002); Proc. SPIE* **4937** 49–61
- [9] Jiang Z, Li M and Zhang X-C 2000 Dielectric constant measurement of thin films by differential time-domain spectroscopy *Appl. Phys. Lett.* **76** 3221–3
- [10] Mickan S P, Lee K S, Lu T M, Munch J, Abbott D and Zhang X-C 2002 Double modulated differential THz-TDS for thin film dielectric characterization *Microelectron. J.* **33** 1033–42
- [11] Mickan S P, Abbott D, Munch J and Zhang X-C 2002 Noise reduction in terahertz thin film measurements using a double modulated differential technique *Fluctuat. Noise Lett.* **2** 13–29
- [12] Mickan S P, Menikh A, Munch J, Abbott D and Zhang X-C 2002 Amplification and modelling of bioaffinity detection with terahertz spectroscopy *Biomedical Applications of Micro- and Nanoengineering (Melbourne, Australia, 2002); Proc. SPIE* **4937** 334–42
- [13] Thrane L, Jacobsen R H, Jepsen P U and Keiding S R 1995 THz reflection spectroscopy of liquid water *Chem. Phys. Lett.* **240** 330–3
- [14] Rønne C, Thrane L, Åstrand P O, Wallqvist A, Mikkelsen K V and Keiding S R 1997 Investigation of the temperature dependence of dielectric relaxation in liquid water by THz reflection spectroscopy and molecular dynamics simulation *J. Chem. Phys.* **107** 5319–31
- [15] Rønne C and Keiding S R 1998 THz reflection spectroscopy of H₂O(l) and D₂O(l) *Ultrafast Phenomena XI (Springer Series in Chemical Physics vol 63)* ed T Elsaesser, J G Fujimoto, D A Wiersma and W Zinth (Berlin: Springer) pp 568–70
- [16] Libon I H, Hempel M, Seitz S, Hecker N E, Feldmann J, Hayd A, Zundela G, Mittleman D and Koch M 1999 THz spectroscopy of polar liquids *Terahertz Spectroscopy and Applications (San Jose, CA, USA, 1999); Proc. SPIE* **3617** 24–9
- [17] Pedersen J E and Keiding S R 1992 THz time-domain spectroscopy of nonpolar liquids *IEEE J. Quantum Electr.* **28** 2518–22
- [18] Kindt J T and Schmuttenmaer C A 1996 Far-infrared dielectric properties of polar liquids probed by femtosecond terahertz pulse spectroscopy *J. Phys. Chem.* **100** 10373–9
- [19] Beard M C, Turner G M, Venables D S and Schmuttenmaer C A 2000 Two-dimensional time-resolved THz spectroscopy of solvent response to photoexcitation *Trends in Optics and Photonics: 12th Int. Conf. on Ultrafast Phenomena* vol 43 (Charleston, SC: OSA) pp 592–4
- [20] Beard M C and Schmuttenmaer C A 2001 Using the finite-difference time-domain pulse propagation method to simulate time-resolved THz experiments *J. Chem. Phys.* **114** 2903–9
- [21] Venables D S, Chiu A and Schmuttenmaer C A 2000 Structure and dynamics of nonaqueous mixtures of dipolar liquids. I. Infrared and far-infrared spectroscopy *J. Chem. Phys.* **113** 3243–8
- [22] Venables D S and Schmuttenmaer C A 2000 Structure and dynamics of nonaqueous mixtures of dipolar liquids. II. Molecular dynamics simulations *J. Chem. Phys.* **113** 3249–60
- [23] Venables D S and Schmuttenmaer C A 2000 Spectroscopy and dynamics of mixtures of water with acetone, acetonitrile, and methanol *J. Chem. Phys.* **113** 11222–36
- [24] Mittleman D M, Cunningham J, Nuss M C and Geva M 1997 Noncontact semiconductor wafer characterization with the terahertz Hall effect *Appl. Phys. Lett.* **71** 16–8
- [25] Asaki M L T, Redondo A, Zawodzinski T A and Taylor A J 2002 Dielectric relaxation of electrolyte solutions using terahertz transmission spectroscopy *J. Chem. Phys.* **116** 8469–82
- [26] Zoidis E, Besnard M and Yarwood J 1996 Far infrared spectroscopic studies of the molecular dynamics and interactions of pyridine in organic solvents *Chem. Phys. Lett.* **203** 233–43
- [27] Rønne C, Jensby K, Loughnane B J, Fourkas J, Nielsen O F and Keiding S R 2000 Temperature dependence of the dielectric function of C₆H₆(l) and C₆H₅CH₃(l) measured with THz spectroscopy *J. Chem. Phys.* **113** 3749–56
- [28] Duvillaret L, Garet F and Coutaz J L 1996 A reliable method for extraction of material parameters in terahertz time-domain spectroscopy *IEEE J. Sel. Top. Quantum Electron.* **2** 739–46
- [29] Mickan S P and Zhang X-C 2003 T-ray sensing and imaging *Int. J. High Speed Electron. Syst.* **13** 601–76
- [30] Born M and Wolf E 1997 *Principles of Optics* 6th edn (Cambridge: Cambridge University Press)
- [31] Arjavalingam G, Pastol Y, Halbout J M and Kopcsay G V 1990 Broad-band microwave measurements with transient radiation from optoelectronically pulsed antennas *IEEE Trans. Microw. Theory Tech.* **38** 615–21
- [32] Duvillaret L, Garet F and Coutaz J L 2000 Influence of noise on the characterization of materials by terahertz time-domain spectroscopy *J. Opt. Soc. Am. B* **17** 452–61
- [33] Mickan S P, Lee K S, Lu T M, Barnat E, Munch J, Abbott D and Zhang X-C 2001 Thin film characterization using terahertz differential time-domain spectroscopy and double modulation *Electronics and Structures for MEMS II (Adelaide, Australia, 2001); Proc. SPIE* **4591** 197–209